Structure and Chirality of the Nematic Phase in α-Chitin Suspensions

E. Belamie,*,† P. Davidson,‡ and M. M. Giraud-Guille†

Laboratoire de Chimie de la Matière Condensée, UMR 7574 CNRS, Université Pierre & Marie Curie, Ecole Pratique des Hautes Etudes, 12 rue Cuvier, Paris, 75005, France, and Laboratoire de Physique du Solide, UMR 8502 CNRS, Université Paris Sud XI, Bât. 510, Orsay 91405 Cedex, France

Received: April 28, 2004; In Final Form: July 6, 2004

We investigate the structure of chiral nematic phases formed by colloidal suspensions of α-chitin rodlike particles in aqueous media. At sufficiently high volume fraction, owing to the particles anisotropic shape, a liquid-crystal phase appears that remarkably mimics the cholesteric geometry observed in biological tissues such as crustacean exoskeletons. The aim of the present work is to describe the structure of chitin colloidal dispersions and the chiral properties of the nematic phase. Both the pH and ionic strength affect the concentrations in the isotropic (C_I) and chiral nematic (C_N) phases at coexistence. The contribution of the crystallites to the ionic strength is evidenced by the linear variation of C_I and C_N with overall chitin volume fraction. When the ionic strength of the solution reaches about 10^{-2} M, the system does not phase separate in bulk anymore; birefringent droplets form throughout the sample but do not coalesce or sediment. SAXS patterns of shear-aligned samples prove the cholesteric nature of the anisotropic phase, previously inferred from optical observations. The liquidlike positional local order, revealed by the presence of broad interference peaks at low angle, is stronger at lower ionic strength. The azimuthal profiles of these patterns allowed us to determine the value of $S \approx 0.8$ of the nematic order parameter at the transition. The cholesteric pitch (P_0) in the biphasic domain of the diagram ranges from 27.5 ± 3.5 μm to 140 ± 17 μm depending on the composition of the suspension medium. The variation of P_0 has been studied as a function of the concentration of crystalline rods in the coexistence domain. Shear-aligned samples were gelled by UV-induced polymerization of acrylamide precursors added to the dispersion medium, thus freezing the alignment. The nematic nature of the gelled samples and their strong shear-induced alignment are confirmed by SAXS.

1. Introduction

Some of the most important biological extracellular matrixes are highly ordered hybrid materials. Connective tissues of vertebrates and arthropod exoskeletons are examples of biological materials in which a fibrous and organized organic matrix serves as a scaffold for the deposition of a reinforcing mineral phase. Collagen fibers in bones and chitin fibers in crustacean shells are both associated with calcium-phosphate and/or -carbonate that diffuse and precipitate after the fibrous component has been excreted and stabilized. In these tissues, the supporting organic component is made of preformed nanometer- to micrometer-size elongated particles that arrange into supramolecular structures with geometries analogous to those of some liquid crystals.[1,2] In compact bones, arthropod cuticles, and plant cell walls, these structures have the macroscopic features of a cholesteric phase, except fluidity. It was shown that, in most cases, the fibers, respectively collagen, chitin, and cellulose, can be extracted from the biological tissues and dispersed in aqueous media to form colloidal suspensions.[3−5] At appropriate concentrations, liquid crystalline phases can be identified, indicating that rodlike, or spindle-like, particles tend to align cooperatively in these systems. Unlike surfactant systems, the particles are rigid and their shape is constant throughout the phase diagram. This makes it easier to understand the influence of different parameters, such as concentration, pH, and ionic strength, on the behavior of the suspensions. Revol and co-workers[3,6−8] clearly showed that suspensions of chitin crystallites form cholesteric phases. This group investigated the effects of pH and ionic strength on the proportion of nematic phase in biphasic samples and found few changes because the contribution of the crystallites themselves is large. Attempts to compare experimental data to theoretical predictions were also made using Onsager's treatment and showed a reasonable qualitative agreement.

The purpose of the present work is to investigate more closely the structure of the suspensions, to establish the nematic nature of the anisotropic phase by probing the liquidlike local order between rods, and to give a quantitative description of the nematic phase chirality. This implies a good knowledge of the thermodynamics of the system and thus we established a full phase diagram in the conditions of pH and ionic strength of interest. We studied the molecular organization and the textures of the nematic phase by small-angle X-ray scattering (SAXS) and polarized light microscopy. We also produced nematic single domains by applying a shear-alignment technique and this alignment could be frozen by UV-induced polymerization of acrylamide precursors. Finally, we compared the structure, thermodynamics, and chirality of the nematic phase with theoretical predictions.

2. Experimental Section

2.1 Extraction and Purification Processes. Chitin flakes extracted from crab shells were kindly provided by Katakura Chikkakin Company, Ltd. (Tokyo, Japan) and France Chitin

* Corresponding author. Tel.: (33)+ 1 44 27 65 52. Fax: (33)+ 1 44 27 65 39. E-mail: ebelamie@snv.jussieu.fr.
† Université Pierre & Marie Curie.
‡ Université Paris Sud XI.

10.1021/jp048152u CCC: $27.50
Published on Web 09/03/2004

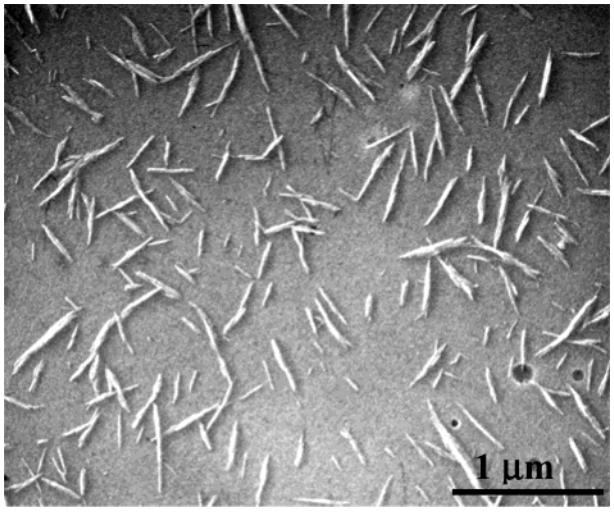

Figure 1. Transmission electron micrograph showing chitin particles shadowed with platinum.

(http://www.france-chitine.com). The particles were prepared mostly following the procedure proposed by Revol et al.[3] One gram of chitin flakes was submitted to hydrolysis in 20 mL of boiling HCl 4 N for 90 min. The resulting suspension was thoroughly dialyzed against deionized water until the pH was more than 3 outside the dialysis bag (Membra-cel, regenerated cellulose; cut-off molecular mass 12−16 kDa, pore size of about 25 Å). After dialysis, the suspension was not yet stable and aggregates remained which tended to sediment. The dispersion of the particles was achieved by sonicating 60 mL aliquots (Branson sonifier) for 1 h (20 kHz, 100 W). Intermittent sonication cycles were used to prevent thermal degradation of the samples, and the effective exposure time was 10% of the total operation time, i.e., 6 min. Large particles and aggregates remaining after the ultrasound treatment were eliminated by low-speed centrifugation (10 000*g*). The supernatants were then spun with an ultracentrifuge at 50 000*g* and the pelleted particles were redispersed in the solvent. This step was repeated at least twice to ensure good exchange of the dispersion medium. Stock suspensions were finally brought to concentrations of about 10% in weight (wt %), measured precisely by drying them and weighing them with a precision scale. The main difference between our preparation process and the one proposed by Revol et al. is that the exchange of the suspending medium and the concentration of the suspensions were achieved by ultracentrifugation rather than dialysis.

2.2 Particles Characterization. *2.2.1 Electron Microscopy.* A transmission electron microscope was used to visualize and measure the dimensions of the chitin crystallites. The samples were prepared following the mica sandwich method: a drop of dilute suspension, at typically 0.003% in weight, was placed between two freshly cleaved mica sheets. The sandwich was opened after about 30 s and the two surfaces were allowed to dry in an oven at 45 °C under vacuum. The particles were shadowed by evaporating Pt at an elevation angle of 10° and then covered with a thin carbon layer. The replicas were recovered by floating the carbon film on a clean water surface and picking up pieces on 300-mesh copper grids. Observations were carried out, either on a JEOL JEM100CXII or a Philips CM12 microscope, at an acceleration tension of 120 kV.

Measurements by TEM of the particles dimensions gave an average length of 260 ± 80 nm and a diameter of 23 ± 3 nm with a rather large polydispersity (Figure 1), based on more than 60 individual measurements.

2.2.2 Titration (Conductimetry/Potentiometry). To determine the particle surface charge density, the total number of ionizable amine groups per particle was estimated following the procedure described by Raymond et al.[9] Chitin suspensions were brought to an appropriate concentration (either 0.6 or 3.1%) with dilute HCl 10^{-4} M and concentrated acid was added in excess (2 mL of 1 N HCl) to ensure complete protonation. Titration was then performed with 0.01 N NaOH and followed simultaneously by potentiometry and conductimetry with a Consort C832 multi-parameter analyzer. Precipitation occurs around pH 6.5, which is also roughly the pK_a of the amine group, and the accurate determination of the volume necessary to titrate the amine groups can prove difficult. Potentiometry is more accurate at higher chitin concentrations, whereas conductimetry is less affected by precipitation at lower volume fractions. We thus performed titrations with suspensions at 0.6 and 3.1 wt % and found consistent values of respectively 1.60×10^{-4} and 1.66×10^{-4} mol NaOH necessary to titrate 1 g of chitin. This corresponds to nearly 1.0×10^{20} amine groups per gram of particles. The surface charge density was then calculated using the average particle volume (1.1×10^5 nm^3), surface (2.0×10^4 nm^2), and density (1.425 g·cm^{-3}) and found to be about 0.76 charge/nm^2, or 15 000 amine groups per particle.

2.2.3 Infrared spectroscopy (FTIR). The degree of acetylation (DA) represents the proportion of glucosamine residues bearing an acetyl group. It is usually close to 100% for chitin and decreases during the acid hydrolysis extraction step. Several methods have been described to evaluate DA, among which the most convenient and easier to perform is infrared spectroscopy. Freeze-dried chitin, with all its groups in the free amino form, was mixed with dry KBr powder to form a platelet. The IR absorption spectrum was recorded on a Magna 550 Fourier transform infrared spectrometer (Nicolet Instrument Corp.), from 500 to 4000 cm^{-1}. It was shown that high DA values are accurately estimated, although slightly underestimated by a few percent at the highest DA, by calculating the ratio of the respective intensities at 1655 and 3450 cm^{-1}.[10−12]

The surface charge density can be deduced from the degree of acetylation (DA) obtained by FTIR, and found to be DA ≈ 75% after the extraction step in concentrated HCl. Note that α-chitin particles are crystallites in which polysaccharide chains are arranged in an antiparallel fashion. If we assume that the hydrolysis of acetyl groups is restricted to the polysaccharide chains directly in contact with the acid, on the surface of the crystallites, then we estimate the number of amine groups per particle to be about 18 000. This is close to but slightly more than the titration results, which possibly arises from underestimation of the DA measured by FTIR by as much as 5%, as shown by comparative NMR studies.[12]

2.3 Sample Preparation. *2.3.1 Dilutions.* Samples were prepared by exchanging the solvent of the stock suspensions with HCl solutions at different concentrations, to which NaCl could be added. We chose not to work with buffered solutions because fluid suspensions could only be obtained at rather low ionic strength. To act as a buffering medium, mixtures of a weak acid and its conjugate base must be more concentrated, by 2 orders of magnitude, than what was acceptable for the system we investigated. We used HCl solutions of concentrations ranging from 10^{-5} M to 10^{-2} M. Their pH was measured by means of a pH meter (Heito) and pH paper (Fisher Scientific) with a 0.2 unit resolution. The pH values of the centrifugation supernatants were also monitored during exchange of the samples. The effect of the ionic strength by itself, beyond that of changes in pH, was tested by adding varying amounts of

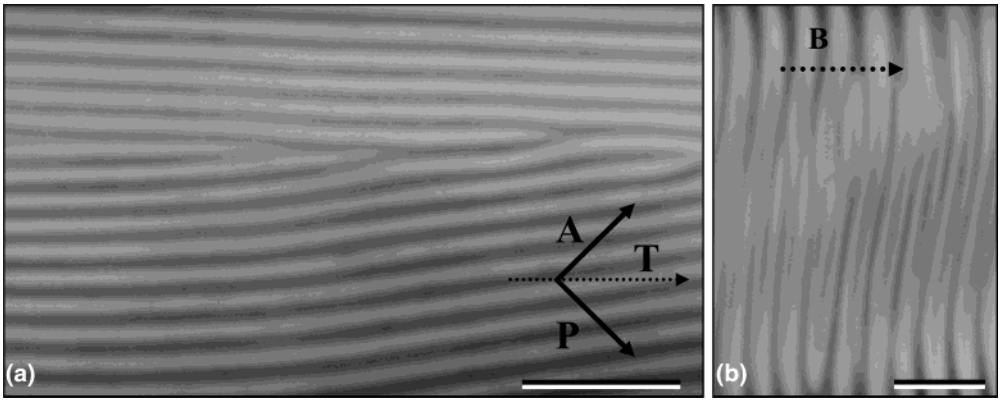

Figure 2. Micrograph showing the fingerprint pattern characteristic of the cholesteric phase as observed between crossed polaroids. For this sample (a), HCl is 10^{-4} M, the chitin concentration is 3.89 ± 0.06 wt %, and $P_0 = 77 \pm 6$ μm. The long axis of the tube (T) is indicated as a horizontal dotted arrow and those of the polaroids are represented as straight arrows making a 45° angle with respect to the tube axis. (b)Same sample with the capillary tube in the same position, after it was kept for 36 h in a 9.4 T magnetic field (B) oriented as indicated by the dotted arrow. Bars: 100 μm.

NaCl to a background 10^{-4} M HCl solution. The salt concentrations were chosen in such a way that the total concentration of mobile ions (Na^+, Cl^-, and H^+), would match those of the corresponding HCl solutions (H^+, Cl^-). For instance, the counterpart of a 2.5×10^{-4} M HCl solution would be a mixture of 10^{-4} M HCl and 1.5×10^{-4} M NaCl.

Concentrated stock suspensions (about 10 wt %) were diluted in small test tubes (6 mm in diameter) by adding the appropriate amount of solvent to reach a given total chitin concentration. These diluted samples were inserted into round glass capillary tubes of 600 μm diameter for microscopic investigations and for more precise determination of the respective volumes of each phase (isotropic/nematic) at coexistence. Note that the choice of rather large round capillaries was dictated by the pitch range of the cholesteric phase, which would have been constrained in flat rectangular capillaries (usually 100 μm thick). The suspensions were sucked into the capillaries. The samples were flame-sealed and stored vertically.

2.3.2 Polyacrylamide Gels. Suspensions of chitin crystallites in HCl 10^{-3} M were mixed with a commercial 30% solution of acrylamide and bis-acrylamide (Sigma) diluted to 10% with HCl 10^{-3} M. The choice of the polyacrylamide system was prompted by the solubility of the monomers (acrylamide and bis-acrylamide) in aqueous media and by the possibility to initiate the polyaddition reaction with a photosensitive reactant. Riboflavine (Vitamin B2) was used as an initiator and since it absorbs light in the near-UV, mixtures appeared yellowish. It was added (1% stock solution in a 50:50 water/ethanol mixture) so that its final concentration was 5×10^{-4} M. The mixtures were then submitted to UV light to initiate polymerization. The time required to complete gelation of polyacrylamide depends on the thickness and nature of the vial walls and the path-length that UV light has to travel. Typically, a UV source (365 nm, 6 W) was shone through flat glass capillary tubes (100 μm thick) overnight. The reaction was started as soon as possible after the mixture was inserted in the tube to maintain the shear-induced alignment.

2.4 Characterization of the Suspension. *2.4.1 Mapping Out the Phase Diagrams.* Observations and measurements were made after the samples had reached equilibrium, which typically took from a few days to up to a year, and after checking that they did not evolve any further. Inspections of the samples were performed between crossed polaroids both with the naked eye and with a microscope. The proportion of nematic phase (X_N) in the coexistence domain was determined as the ratio of the distances between the bottom of the tube and respectively the I/N interface and the air−liquid meniscus.

2.4.2 Optical Microscopy in Polarized Light. Measurements of the chiral nematic pitch (P_0) were also performed with round capillary tubes. They were covered with water to limit optical distortion due to the large difference in refractive indices between air and glass, and all P_0 values were measured in the same conditions. The observations were done between crossed polarizers on a Nikon Eclipse E600Pol microscope, equipped with a DXM 1200 CCD camera to capture high-resolution pictures. Each value reported for P_0 in a given set of conditions is an average taken over 10−50 independent measurements along at least two different capillaries.

2.4.3 SAXS Experiments. Small-angle X-ray scattering (SAXS) experiments were performed on the D24 experimental station of the LURE synchrotron facility. The D24 setup has already been described in detail.[13] The Ge(111) monochromator provides an X-ray beam focused in the horizontal plane, with a flux of about 10^{10} photons/s·mm^2 and a wavelength $\lambda = 1.488$ Å. The beam path is kept under vacuum and antiparasitic slits are placed before the sample to reduce background noise. The scattered X-ray intensity was recorded using imaging plates. The sample−detector distance was 2.70 m and typical exposure times were 10 min. Samples of the liquid-crystalline phase were aligned by sucking material into flat optical capillary tubes (VitroCom, Mountain Lakes, NJ). Despite the strong absorption (90−95%) due to the glass walls, this technique was chosen because it is known to provide very well-aligned samples.[14] Recording of the diffraction patterns was started as soon as possible after the sample was prepared and sealed.

3. Results

In the following we first present the structural work on the macroscopic chirality of the nematic phase and its microscopic organization. Then, we report our data regarding the thermodynamics of the phase transition, and in particular the phase diagrams on which the structural work was based.

3.1 Chiral Nematic Phase. *3.1.1 Optical Microscopy.* Cholesteric Pitch. One important parameter that characterizes the chirality of the cholesteric phase is its pitch (P_0), commonly defined as the distance that separates rods of same orientations after 360° rotation. In practice, we measured the distance between successive extinction lines (Figure 2), corresponding to homeotropic orientations of the rods (parallel to the optical axis), and equal to $P_0/2$. Note here that the pitch measurements

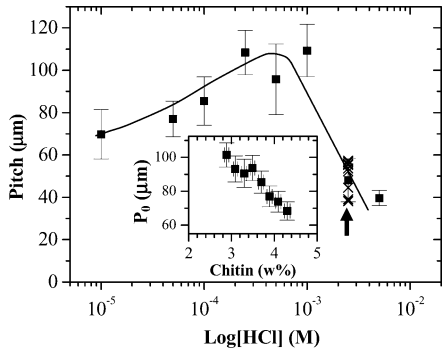

Figure 3. Variation of the average cholesteric pitch in biphasic samples prepared at different HCl concentrations. Each data point is the average value of data taken along a dilution series in the biphasic domain. The entire set of pitch values is shown for HCl = 2.5×10^{-3} M (crosses). The line is a guide to the eyes. The inset shows the evolution of the pitch as a function of chitin concentration for the case where HCl = 10^{-4} M. Every pitch value reported in the graph is an average taken over 10−50 measurements made along the capillary tube axis.

in the chiral nematic phase were restricted to samples at coexistence because the winding up of the cholesteric phase did not occur at higher concentrations. Nevertheless, the evolution of P_0 as a function of HCl concentration (for cholesteric samples at coexistence) is plotted in Figure 3 and appears to be nonmonotonic. Each data point is the average over all the values measured in a dilution series for a given condition (HCl concentration). We show the entire set of values corresponding to a dilution series at a HCl concentration of 2.5×10^{-3} M as black crosses spread around the mean value (black square). This nonmonotonic dependence is probably related to the re-entrance displayed by the phase diagram (see Figure 10 below).

In the coexistence domain, the value of P_0 in the cholesteric phase is not constant but decreases as the total chitin concentration in the sample increases, as shown in the inset in Figure 3.

Shearing and Polyacrylamide Gels. We observed that, just after preparing capillaries by sucking in nematic dispersions, the samples appeared strongly aligned when seen between crossed polaroids. However, this spontaneous alignment induced by shear relaxes in a matter of hours at most as the twist elasticity winds up the chiral nematic texture, thus suppressing the alignment. To maintain and lock the alignment, samples were prepared with the aim of embedding the liquid crystal in a gelled matrix. The pictures shown in Figure 4 were taken days after the samples were prepared and submitted to UV light. At the same chitin concentration, samples prepared in HCl do not exhibit any particular orientation (Figure 4 a and b), whereas mixtures with acrylamide precursors and riboflavine have kept the alignment initially induced by shear (Figure 4 c and d). Indeed, the latter samples are strongly birefringent when the tube axis makes an angle of 45° with the orientations of the polarizer (P) and the analyzer (A). In contrast, they appear dark when the tube axis is aligned with P or A. Insertion of a quarter-wave plate shows that the slow axis of the phase is parallel to the tube axis, and thus the chitin rods are also aligned in this direction.

3.1.2 Small-Angle X-ray Scattering. Figure 5 shows the SAXS patterns of various samples of the cholesteric phase aligned by shear flow (see the Experimental Section). As inferred from observations by optical microscopy in polarized light, the SAXS patterns are very anisotropic, which proves that the helical organization was completely unwound by the shear and that the phase remained aligned during the SAXS experiment (typically 10 min). These scattering patterns are typical of

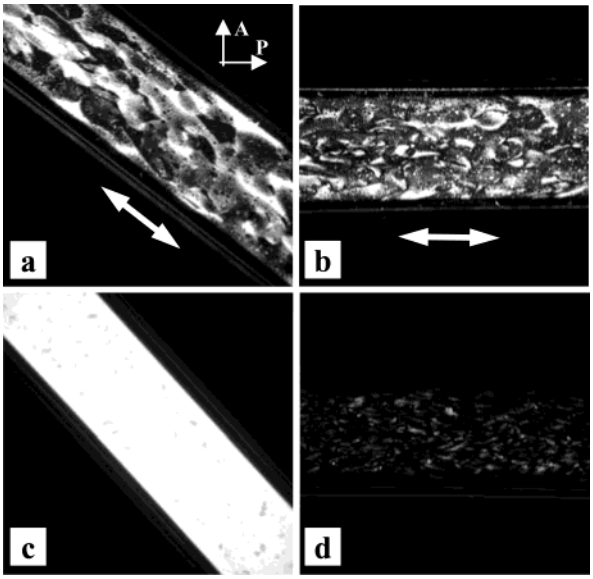

Figure 4. Micrographs, taken in flat capillaries between crossed polaroids, of 4.5 wt % chitin suspensions with acrylamide precursors. In one case (pictures c and d), Riboflavine was added to initiate polymerization under UV light. The shear alignment is evidenced by the strong difference in birefringence for the two orientations in c and d. White double-headed arrows indicate the tube orientation; those of the polaroids are labeled A and P.

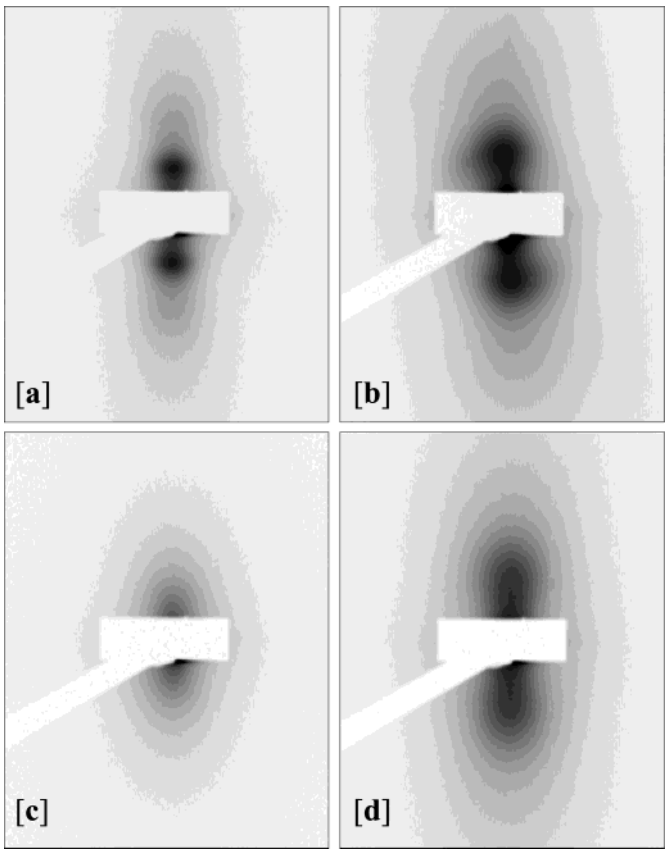

Figure 5. SAXS patterns obtained with suspensions at different chitin and HCl concentrations: (a) HCl 10^{-3} M, chitin 6 wt %; (b) HCl 10^{-3} M, chitin 10.5 wt %; (c) HCl 10^{-2} M, chitin 6 wt %; and (d) HCl 10^{-2} M, chitin 13.5 wt %.

lyotropic nematic suspensions of rodlike particles.[15−21] At low ionic strength (Figure 5 a and b), two diffuse spots are observed in the vertical direction. They classically represent the intersection with the Ewald sphere of a diffuse scattering torus that arises from interferences among rods in planes perpendicular

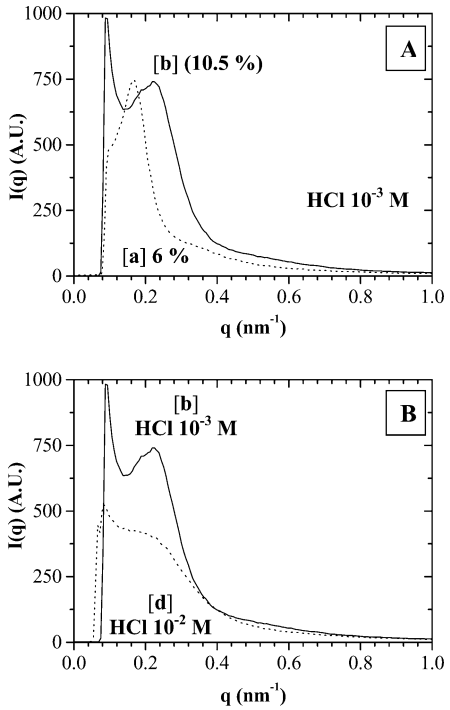

Figure 6. Radial scans of the scattered intensity, as a function of scattering vector modulus q, going through the diffuse spots, from the patterns shown (and labeled as) in Figure 5. The top figure (A) compares profiles obtained in HCl 10^{-3} M with 6% and 10.5% chitin, and the bottom one (B) shows the broadening of the peak for 6% chitin suspensions when the HCl concentration goes from 10^{-3} M to 10^{-2} M.

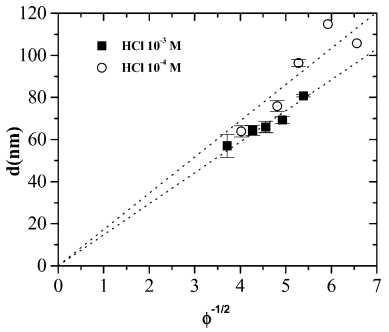

Figure 7. Dilution law: distance between particles d (nm) deduced from SAXS patterns as a function of $\phi^{-1/2}$, the inverse square root of the chitin volume fraction in the cholesteric phase.

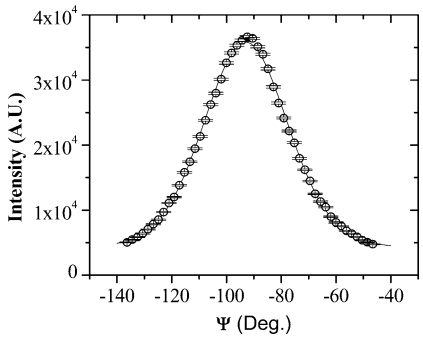

Figure 8. Typical azimuthal profile of aligned SAXS patterns recorded along a circle of constant q-value going through the maximum of the diffuse spots. The solid line is a fit performed to extract the nematic order parameter (see text for details).

to the nematic director. This immediately tells us that the chitin rods are horizontally aligned, i.e. parallel to the shear flow, as intuitively expected. The radial scans of the scattered intensity through the diffuse spots display broad peaks that are due to a short-range liquidlike positional order (Figure 6).

Let us first describe the liquidlike positional order. The position in q-space (q is the scattering vector modulus defined by $q = 4\pi/\lambda \sin\theta$ where 2θ is the scattering angle and λ is the wavelength) of the diffuse peaks corresponds to the average distance d (typically 60−120 nm) between chitin particles in planes perpendicular to the director. The liquidlike order is stronger at low ionic strength (compare profiles in Figure 6 B) because it is most probably due to electrostatic repulsive interactions that are screened at high ionic strength. In fact, the diffuse scattering peaks completely disappear at high ionic strength, and the scattered intensity regularly decays with scattering vector modulus. Such a behavior is very common with electrostatically-stabilized colloids. The width (fwhm) of the diffuse peak provides a rough estimate of the correlation length ξ over which the liquidlike order extends. ξ is actually rather small in this system and never takes values larger than about 150 nm, which corresponds to a local positional order extending only over the next neighbor particles. The average distance, d, between particles depends, of course, on chitin concentration or, more conveniently, on its volume fraction, ϕ. For a nematic phase of very anisotropic rodlike particles, this dependence, also called "swelling law", is of the form: $d = k\phi^{-1/2}$.[22−24] Despite the rather limited range of volume fraction that could be explored, it is clear that liquid-crystalline chitin suspensions follow this swelling law (Figure 7). There are small differences between dilution lines located at low and high ionic strengths but these differences are not significant. (At high ionic strength, the peaks are much broader and the positions of their maxima are difficult to determine accurately.) If a local 2D hexagonal packing of the particles is further assumed, then the prefactor k (i.e., the slope) of the swelling law can be related to the chitin particle diameter D: $k = (\pi\sqrt{3}/8)^{1/2} D = 0.825D$. This geometrical reasoning relates the rods volume fraction to the average distance between their centers of mass and provides us with an estimate of the chitin crystallite diameter $D \approx 20$ nm in good agreement with the values obtained from electron microscopy images.

We now turn to the long-range orientational order. As mentioned above, applying a shear flow was found to be a very efficient way of unwinding the cholesteric helices and aligning the chitin particles. Then, the samples can be considered as nematic single domains. There are several, more or less equivalent, ways of deriving the nematic order parameter S from the scattering patterns of aligned samples.[16,25,26] We use here the approach of Leadbetter et al. that relates the azimuthal profile of the SAXS pattern (Figure 8), recorded along a circle of constant q-modulus going through the maximum of the diffuse spots, to the orientational distribution function (odf) and ultimately to S. Moreover, if one assumes the classical Maier-Saupe form for the odf, then S is easily obtained by a fit of the azimuthal profile.[27−29] The best aligned samples gave rather high values of $S \approx 0.8$, in good agreement with the Onsager model.[30,31] Note that after times ranging from several minutes to months, depending on concentration, the alignment vanishes and the SAXS patterns progressively lose their anisotropy.

The alignment of chitin crystallites induced by shear flow could be effectively frozen by acrylamide polymerization. This was demonstrated by preparing two batches of the same chitin suspension and incorporating acrylamide in only one of them. Then, shear-aligned samples, held in flat glass capillaries, were produced with both batches. The acrylamide-containing sample was polymerized with UV light and the samples were then left to relax for 24 h. Figure 9 illustrates the comparison between

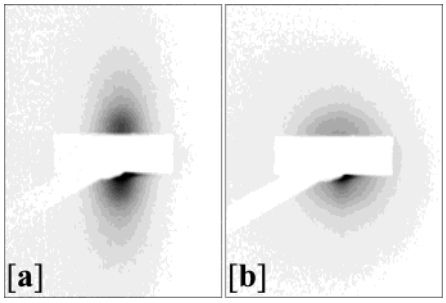

Figure 9. SAXS patterns obtained with suspensions aligned in flat capillaries and frozen by acrylamide polymerization under UV. The samples used to take patterns a and b correspond to those seen in polarized light in Figure 6 c and d and a and b, respectively.

the SAXS patterns of the fluid and the gelled samples. Obviously, the sample gelled with polyacrylamide has retained its orientational order whereas the other one has not, which confirms our previous optical observations. Recently, Nge et al. were able to mix chitin suspensions with acrylic acid[32] that could be polymerized under UV, in a way similar to the procedure we followed here. Polymerization was induced after the samples were submitted to either shearing or a magnetic field. The crystallites' orientation was determined by wide-angle X-ray scattering (WAXS)[33] on the dry solids obtained after water evaporation, and not on the nematic phase itself. The authors showed that in the resulting solid the crystallites are aligned perpendicular to the magnetic field direction, suggesting that this orientation is inherited from the fluid phase. A comparable behavior has been reported for cellulose whiskers in a very similar experiment not only on dry magnetically aligned particles,[34] but also in the fluid state.[35] In our study, the nematic phase was shear-aligned in the fluid state, the uniaxial orientation was locked by UV-induced acrylamide polymerization, and placed as is in the synchrotron beam, in this highly diluted state.

3.2 Phase Diagrams. Dilute colloidal suspensions of chitin microcrystals are isotropic and show no birefringence when viewed in polarized light between crossed polaroids. For concentrations above a critical value C_I, an ordered cholesteric N* (chiral nematic) phase appears, with concentration C_N. This phase is birefringent and shows a typical fingerprint pattern as in Figure 2. The isotropic and chiral nematic phases coexist throughout an extended biphasic domain. This clearly demonstrates that the phase transition is first order, and that the suspensions have reached thermodynamic equilibrium. The main features of the phase diagrams mapped out in the present study are in agreement with previous work.[3,6] A set of capillaries, representing a dilution series in the coexistence domain was kept for several weeks at different temperatures between 4 and 100 °C. The proportion of the nematic phase did not change in any sample. No influence of temperature was thus observed in this very sensitive experiment, implying that the system is essentially athermal. The isotropic phase, which is dark at rest when viewed between crossed polaroids, becomes very bright when gently shaken. This large flow birefringence decays in less than a second.

When placed in a magnetic field, both isolated birefringent droplets, also called tactoids, and the continuous chiral nematic phase align with the cholesteric axis parallel to the field. The photograph in Figure 2 b was obtained with a sample kept in a 9.4 T magnetic field for 36 h and observed immediately after taking it out. The alignment of the nematic phase in the magnetic field was also checked by WAXS where the Bragg reflections from the polysaccharides crystal lattice are used to evidence the anisotropic orientation of the crystallites (data not shown).

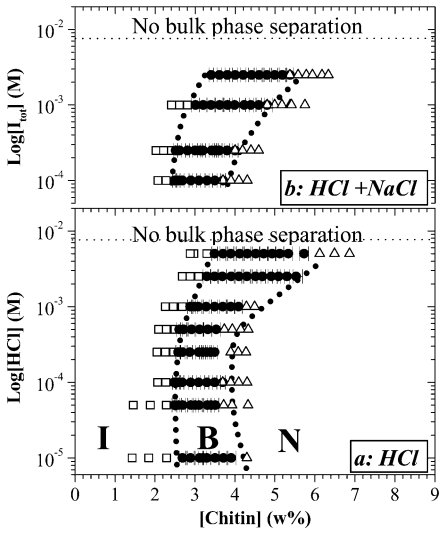

Figure 10. Phase diagrams obtained for chitin elongated particles, mapped out by visual inspections of samples with different chitin concentrations between crossed polaroids. Open square, isotropic; solid circle, biphas; open triangle, chiral nematic. (a) Dispersions in a series of HCl solutions. No bulk phase separation was observed for samples at HCl = 10^{-2} M and beyond. (b) Dispersions in HCl 10^{-4} M to which various amounts of NaCl were added. I_{tot} refers to mobile ions added to the suspensions and is thus the sum of HCl and NaCl concentrations. For samples prepared with $I_{tot} > 5 \times 10^{-3}$ M, no bulk phase separation was observed. (Measurements were made at room temperature; however, the system was found to be athermal).

3.2.1 Phase Diagram as a Function of HCl Concentration. The samples in test tubes were observed between crossed polarizers with the naked eyes. The results of these visual inspections are reported in Figure 10 a and b. For HCl concentrations between 10^{-5} M and 5×10^{-4} M and chitin concentrations below 2.5 wt %, the samples remain completely isotropic and show no birefringence. Beyond 2.5 and up to 4 wt % chitin, the liquid appears bright in polarized light, and within a few days, a birefringent phase settles at the bottom of the tubes, separated from an upper isotropic one by a sharp interface. When the chitin concentration is further increased, the samples are entirely anisotropic. The boundaries of the biphasic domain only slightly change in this HCl concentration range (Figure 10 a). Both C_I and C_N increase when the HCl concentration increases from 5×10^{-4} M to 2.5×10^{-3} M. Samples of HCl molarity larger than 2.5×10^{-3} M but lower than 10^{-2} M only showed complete phase separation in the biphasic gap at low values of C_{tot}. Samples prepared with 10^{-2} M HCl and beyond never exhibited bulk phase separation, in test tubes, in the whole range of chitin concentration investigated. Instead, the birefringence increased continuously from dark to very bright samples when viewed between crossed polaroids. Observations with a polarizing microscope revealed the presence of very small birefringent droplets that grow in size, without either merging with each other or sedimenting, eventually leading to a continuous highly defected nematic phase. In contrast with the other samples, these suspensions do not flow spontaneously when tilting the test tubes. Both these microscopic and macroscopic observations suggest the formation of a weak physical gel.

3.2.2 Phase Diagram as a Function of NaCl Concentration. Samples were prepared with a background HCl concentration of 10^{-4} M to which various amounts of NaCl were added. The total ionic strength, I_{tot}, refers to mobile ions added to the suspensions and is thus essentially the sum of HCl and NaCl concentrations. As I_{tot} increases (Figure 10 b), C_I and C_N follow

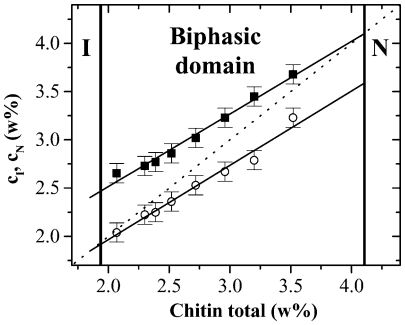

Figure 11. Coexistence concentrations C_I and C_N, of the isotropic and nematic phases, respectively, measured with a series of samples prepared in the biphasic domain. As the total chitin concentration is increased, both C_I and C_N increase. For a given total chitin concentration, each set of concentrations C_I and C_N is those of the phases in equilibrium. The vertical straight lines mark the boundaries of the biphasic domain as in Figure 10. The oblique straight lines are linear fits to C_I and C_N. (Measurements were made at room temperature; however, the system was found to be athermal).

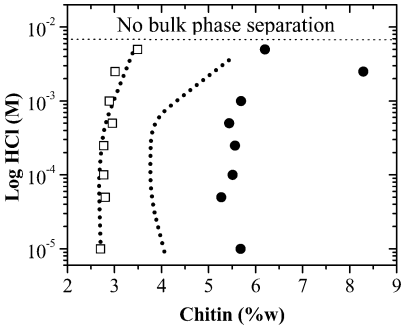

Figure 12. Comparison between boundaries of the biphasic domain determined by visual inspection in large tubes of 6 mm in diameter as in Figure 2 (boundaries drawn as dotted lines), and by linear extrapolation of the proportion of nematic phase measured in capillary tubes (open square, I/B boundary; solid circles, B/N boundary). All measurements were made after the tubes had been left standing for several months at room temperature. Beyond an HCl concentration of 5×10^{-3} M, no phase separation was observed. (Measurements were made at room temperature; however, the system was found to be athermal).

exactly the same trend as with HCl only. The two different kinds of phase diagrams actually superimpose quantitatively. This shows that the phase separation is mostly sensitive to ionic strength, more than pH.

3.2.3 Nematic Phase Volume Fraction as a Function of Chitin Overall Concentration. The proportion of nematic phase X_N increases with total chitin concentration, and extrapolations of X_N to 0 and 1 respectively give the concentrations in the isotropic (C_I) and nematic (C_N) phases. In principle, this is true only if X_N varies linearly with the total chitin concentration. We measured the actual concentrations in both phases for a series of samples in the biphasic gap in HCl 10^{-4} M. Note that, considering the large volumes of suspension required to make accurate concentration measurements by drying and weighing, a different batch of chitin suspension was prepared for this purpose. Figure 11 shows that, in the biphasic gap, both C_I and C_N increase linearly as a function of the total chitin concentration. The intersection with the diagonal gives boundary concentrations for the biphasic gap of 1.85 and 4.1 wt %.

The extrapolated coexistence concentrations measured in 600 μm capillary tubes are reported in Figure 12 together with the boundaries observed visually in 6 mm test tubes. Whereas the values for C_I are very similar in all experimental conditions, oddly enough the concentrations of the biphasic/nematic boundary C_N do not match and seem to depend strongly upon the tube diameter.

4. Discussion and Conclusions

4.1 Structure and Thermodynamics of the Nematic Phase. Altogether, SAXS experiments demonstrate that chitin microcrystals suspensions have a nematic-type organization beyond a critical volume fraction, as inferred from previous results.[3,6−8] In most cases, the system rapidly reaches thermodynamic equilibrium and exhibits a coexistence domain throughout which the two phases, isotropic and chiral nematic, are separated by a sharp interface, indicating a first order transition. The anisotropic phase has a high order parameter, as measured by SAXS. The cholesteric chirality is only a small perturbation to nearest neighbors interactions and the phase behaves mostly like a real nematic (i.e., achiral). Most of the time, diffraction peaks, due to positional local order, are observed at q-values corresponding to interparticle distances ranging from about 60 to more than 100 nm. The particles being about 20 nm in diameter, their surfaces are separated by a distance of at least 40 nm (two bare diameters) and thus mostly interact through the uttermost part of the counterions diffuse layer. The presence of correlation peaks also indicates that attractive long-range interactions, if any, do not dominate. In addition, as expected, the system is essentially athermal in a temperature range from 4 to 100 °C.

Models have been developed and refined since Onsager's work in order to predict the behavior of an assembly of rods dispersed in a solvent.[31] More recently, another expression of the free energy of spherocylinders suspensions was proposed by Lee[36] to describe the transition for particles of low aspect ratio. It is a generalization of the Carnahan−Starling equation for the free energy of a hard sphere fluid to the case of a nematic liquid crystal in which orientation degrees of freedom are decoupled from translational ones. The numerical simulations and Lee's theory are in very good agreement and converge with Onsager's model for high aspect ratios. In the following discussion, we will examine to what extent suspensions of chitin microcrystals in HCl solutions can be described by these theoretical models. We calculate coexistence concentrations assuming a purely entropy-driven phase separation. Chitin suspensions are stabilized versus flocculation by charges arising from the protonation of amine groups present on the surface of the crystallites. The clouds of counterions and co-ions surrounding the rods are responsible for an apparent increase in diameter, function of the Debye length κ^{-1}. The volume from which one rod is excluded due to the presence of its neighbor (excluded volume) is thus proportional to an effective diameter D_{eff} that is affected by the surface charge density and the total ionic strength of the suspension. These two parameters can hardly be measured directly. As presented in the results section, we calculated a "bare" charge density σ_{bare} of about 0.76 charges/nm^2, based upon titration and infrared spectroscopy, which is slightly more than the values of 0.5 and 0.6 found by Revol et al. with two different colloidal suspensions.[6] The contribution of the crystallites to the total ionic strength was included and the surface charge density was varied relative to the pH of the suspension, considering the pK_a of the amine group to be 6.3.[6] The effective linear charge density λ_{eff}^{sat} was estimated using the analytical approximation proposed by Aubouy et al.[37] The volume fractions at coexistence ϕ_i and ϕ_n were then calculated according to Onsager[30,31] and Lee.[36] Details of the calculations can be found in the appendix.

The contribution of the crystallites to the total ionic strength is not negligible, especially at low HCl concentrations. For

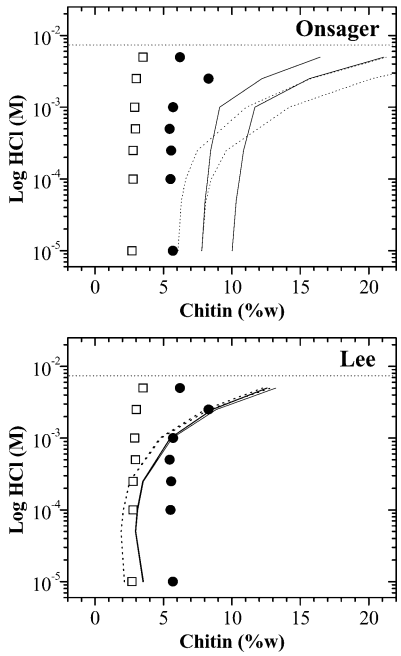

Figure 13. Experimentally measured coexistence concentrations, plotted together with predictions given by Onsager's (a) and Lee's (b) models for two total chitin concentrations (3 and 6 wt %) and for a series of HCl concentrations. The dotted lines correspond to a total chitin concentration C_T of 3 wt %, and the solid lines correspond to C_T = 6 wt %. Both models predict that the coexistence concentrations are higher at 6 wt % than at 3 wt % at low ionic strength. The open squares and solid circles are the coexistence concentrations measured by extrapolation, taken from Figure 12.

instance, with HCl = 10^{-5} M, κ^{-1} varies from 25.3 to 13.3 nm, as the chitin concentration increases from 2 to 10% and consequently D_{eff} decreases by a factor of 2. However, with HCl = 10^{-3} M, κ^{-1} only goes from 12.5 to 9.5 nm in the same interval. The coexistence concentrations being directly related to D_{eff}, the influence of the chitin particles concentration is much more important at low HCl concentrations. This effect of the crystallites contribution to the ionic strength and hence to D_{eff}, is evidenced in Figure 5 where the coexistence concentrations ϕ_i ($\boldsymbol{C}_\mathbf{I}$) and ϕ_n ($\boldsymbol{C}_\mathbf{N}$) increase with the total chitin concentration.

The concentrations predicted with Onsager's model, plotted together with the experimental data in Figure 13 a, miss the experimental data by more than a factor of 2. The same discrepancy was reported for similar systems, like TMV for instance.[38] Predictions according to Lee's model are shown on a similar graph in Figure 13 b and fall in a range of chitin concentration more consistent with experiments. The predicted coexistence volume fractions (ϕ_i, ϕ_n) become almost equal at low aspect ratio, in our case at low HCl and chitin concentrations. The width of the coexistence domain, given by the ratio $\boldsymbol{C}_\mathbf{N}/\boldsymbol{C}_\mathbf{I}$ (ϕ_n/ϕ_i), has been predicted between about 1.1 to 1.34 by different treatments.[30,31,36] The boundaries of the biphasic domain in Figures 10 and 12 reflect the variations of the coexistence concentrations as a function of HCl, NaCl, and chitin concentrations. The ratio of chitin concentrations at these boundaries *I*/*B* and *B*/*N* is about 2. Figure 11 shows that for each set of HCl and chitin concentrations in the biphasic gap, the coexisting concentrations are much closer, with a ratio $\boldsymbol{C}_\mathbf{N}/\boldsymbol{C}_\mathbf{I}$ of about 1.2, very close to the value of 1.1 predicted by Lee's model for $L/D \approx 15$.

The contribution of the chitin particles to the ionic strength is illustrated for both models in Figure 13 a and b, with sets of ϕ_i and ϕ_n calculated at 3 and 6 wt % total chitin concentration. The biphasic gap is thus broadened due to the fact that the volume fraction of chitin in the coexisting phases increases with its overall concentration in the sample. In the lower part of the diagram, Lee's model captures qualitatively the evolution of ϕ_n, especially its slightly re-entrant character.

The upper part of the phase diagram clearly shows a departure from the model, probably because a weak physical gel forms at higher ionic strength, which hinders the sedimentation of the nematic droplets and hampers the bulk phase separation. Indeed, despite their larger density, nematic droplets imbedded within the isotropic phase do not sediment on a time-scale of months, which indicates the existence of a yield stress. Actually, this is not too surprising since the literature abounds in systems of anisotropic moieties that display both gel and liquid-crystalline properties.[39−47] Similar tactoids were described in an early work on V_2O_5 suspensions.[48] The physical origin of the gelation is not well understood, all the more since it may involve several different mechanisms depending on the kind of microscopic interactions at work (repulsive gels, attractive gels, different kinds of percolation, etc.[49,50]). In the case of a purely steric, excluded-volume interaction, experiments with model systems[51,52] have shown that the volume fraction at which gelation occurs scales as the inverse of the aspect ratio, just like the Onsager threshold for nematic ordering. Then, molecular details will determine where the gelation threshold is located with respect to the isotropic/nematic coexistence region. In chitin suspensions, gelation seems to occur in the biphasic gap, close to the nematic boundary, a situation comparable to that of boehmite suspensions in cyclohexane.[53] Note that this weak physical gel easily aligns under shear flow but it is still strong enough to prevent formation of clear cholesteric textures, thus hampering pitch measurements beyond 6.5 wt %.

4.2 Chirality of the Nematic Phase. The origin of macroscopic chirality in cholesterics is still a much debated question. The most commonly accepted picture is that for threaded rods interacting with electrostatic repulsions, the most favorable situation is when the axis of one rod aligns with the groove of the neighboring one. According to some theories,[54,55] the scaling law $P_0 \propto c^{-\nu}$, that relates P_0 with the concentration of rods, involves an exponent $\nu = 1$ for hard chiral rods and $\nu = {}^5/_3$ for semi-flexible chiral chains. However, Pelcovits predicts a value of $\nu = 2$, independent of the chain flexibility.[56] More recently, other attempts were made to take into account details of the helical charged pattern and relate it to the macroscopic pitch through chiral electrostatic interactions.[57,58]

We find that for a given HCl concentration, for instance10^{-4} M, P_0 decreases in the coexistence domain. We know from direct measurements that the concentration of chitin in the nematic phase increases with the overall concentration of particles. This shows that the pitch of the cholesteric phase decreases as the particle volume fraction increases in the nematic phase. The decrease in P_0 as a function of chitin volume fraction gives straight lines in log−log plots with an exponent that increases with HCl concentration. However, direct representations of P_0 as a function of chitin concentration also give straight lines, and thus the exponents measured on logarithmic plots are not significant enough to discriminate between available models for the origin of the nematic phase long-range helicity. We note that our values, taken at low ionic strength, extend those of Dogic and Fraden for fd virus[59] in Tris-HCl buffers and at higher salt concentrations. We measured exponents ranging from roughly 0.3 to 1.0 in HCl 10^{-5} M to 5×10^{-3} M and Dogic et al. found values ranging between 1.0 and 1.6 in 5×10^{-3} M to 10^{-1} M Tris buffers.

Extremely different situations have been reported for DNA that shows no variation of the pitch as a function of concentration[60] or to the contrary a strong dependence,[61] and for PBLG in dioxane that has $\nu = 2$.[62] Moreover, a number of other different values are available throughout the literature for similar systems. A recent work with PEG-grafted fd viruses[63] shows variations of the pitch with ionic strength, even when the effective diameter due to electrostatic repulsions is smaller than bare diameter plus the polymer-grafted layer. The evolution of the cholesteric pitch in chitin suspensions is clearly related to changes in D_{eff} as a function of the total ionic strength. The fact that chitin crystallites are rigid particles simplifies the problem, compared to that of semi-flexible rods such as fd virus, DNA, or collagen. However, a better analysis of chitin suspensions chiral behavior will require a complete study over a wide range of concentration in the pure cholesteric phase.

4.3 Conclusions. In the first part of this publication, we investigated the macroscopic organization of the cholesteric phase, and in particular its chirality, by studying the evolution of the pitch as the composition of the mixtures changes. We then studied the microscopic structure of the nematic phase by probing the liquidlike local order by SAXS. This structural work implied a good knowledge of the system thermodynamics. We thus reported a phase diagram of these chitin suspensions for concentrations ranging from 1 to 7 wt % and ionic strength ranging from 10^{-5} M to 10^{-2} M, with data indicating that the system exhibits a bulk phase separation in a large pH range but at rather moderate ionic strength. The proportions of the two phases at coexistence were measured for a series of aqueous solutions of increasing HCl concentrations. Finally, we discussed the relevance of classical theories to model the behavior of this system and compared their predictions to experimental findings. Reaching a good description of the phase diagram and a better understanding of the underlying mechanisms makes it easier to control the behavior of the suspensions as a function of concentration, pH, ionic strength, mixing with other chemical species, and applying external fields, such as shearing for instance. Chitin suspensions can prove to be a useful model to study electrostatically stabilized colloidal systems, thanks, for instance, to the particles' thermal stability and the possibility to disperse them in acidic solutions but also in non-aqueous media.

Appendix

The Debye length is calculated using the following formula:[64]

$$\kappa^{-1} = [4\pi l_B(2n_s + n_P\Gamma\alpha Z_P)]^{-1/2}$$

with l_B the Bjerrum length (0.714 nm in water at 25 °C); n_s the number density of each mobile ion; n_p the particles concentration, Z_p the total number of charges per rod; α, the fraction of ionized groups at a given pH; and Γ, the Donnan salt exclusion coefficient that depends on the linear surface charge density λ_{eff} and is calculated according to Manning:[65]

$$\lim_{n_s \to 0} \Gamma = \frac{1}{2}\left(1 - \frac{1}{2\xi}\right),\ \xi < 1$$

$$= (4\xi)^{-1},\ \xi > 1$$

$$\text{with } \xi = \lambda_{\text{eff}} \times l_B$$

The bare linear charge density on the surface of the particles, λ_{bare} is related to the surface charge density: $\lambda_{bare} = 0.93\sqrt{\sigma_{bare}}$

At this point, one needs to evaluate the effective charge density which takes into account nonlinear screening effects owing to the presence of counterions close to the surface. To this purpose we used the analytical approximation proposed by Aubouy et al.[37] that saturates at high bare charge density: $\lambda_{eff}^{sat} l_B = \kappa D_{bare} + 3/2$ and is good for $\kappa D_{bare}/2 \geq 1$.

The classical treatment to calculate D_{eff} then follows:

$$D_{eff} = D_{bare} + \kappa^{-1}(\ln A' + C_E + \ln 2 - 1/2)$$

with $A' = \pi(\lambda_{\text{eff}}^{\text{sat}})^2 4 l_B^2 e^{-\kappa D_{\text{bare}}}/2\kappa l_B$, and $C_{\text{E}} = 0.577$ is Euler's constant.

We see with the above set of equations that the effective linear charge density λ_{eff}^{sat} evolves with κ, which in turn is a function of the effective number of charges carried by the rods. Iterative calculations of λ_{eff}^{sat} were performed until the difference between successive estimates of D_{eff} was less than 0.1%.

The volume fractions at coexistence ϕ_i and ϕ_n were then calculated according to Onsager[30,31] and Lee:[36]

$$\phi_{i,n}^{Ons} = K_{i,n}{}^1[(1 - K_{i,n}{}^2 h) \times b]^{-1},$$

$b = \pi L^2 D_{eff}/4$ and $h = 1/\kappa D_{eff}$ is the twisting parameter that is actually negligible here. L is the length of the particles. Constants $K_{i,n}^{1,2}$ are taken from the literature: $K_i^1 = 3.290$, $K_n^1 = 4.191$, $K_i^2 = 0.675$, $K_n^2 = 0.730$.

$$\phi_{i,n}^{Lee} = \frac{\eta_{i,n}}{\pi D_{eff}{}^2 L/4},$$

$\eta_{i,n}$ is taken from Lee et al.,[36] with an effective aspect ratio $x_{eff} = 1 + L/D_{eff}$.

Volume fractions ϕ are converted into percent weight concentrations $C_{\%}$ in the graphs:

$$C_{\%} = \frac{100\phi D_{bare}{}^2 \pi L d}{4 - \phi D_{bare}{}^2 \pi L(1 + d)}$$

where d is the chitin crystallites density (1.425 g·cm^{-3}).

References and Notes

(1) Bouligand, Y. *Tissue Cell* **1972**, *4*, 189.
(2) Neville, A. C. *Insect Ultrastructure*; Blackwell Scientific Publications: Oxford, Edinburgh, 1970.
(3) Revol, J.-F.; Marchessault, R. H. *Int. J. Biol. Macromol.* **1993**, *15*, 329.
(4) Giraud-Guille, M.-M. *J. Mol. Biol.* **1992**, *224*, 861.
(5) Revol, J.-F.; Bradford, H.; Giasson, J.; Marchessault, R. H.; Gray, D. G. *Int. J. Biol. Macromol.* **1992**, *14*, 170.
(6) Li, J.; Revol, J.-F.; Naranjo, E.; Marchessault, R. H. *Int. J. Biol. Macromol.* **1996**, *18*, 177.
(7) Li, J.; Revol, J.-F.; Marchessault, R. H. *J. Colloid Interface Sci.* **1996**, *183*, 365.
(8) Li, J.; Revol, J.-F.; Marchessault, R. H. *J. Appl. Polym. Sci.* **1997**, *65*, 373.
(9) Raymond, L.; Morin, F. G.; Marchessault, R. H. *Carbohydr. Res.* **1993**, *24*, 331.
(10) Domzy, J. G.; Roberts, G. A. F. *Makromol. Chem.* **1985**, *186*, 1671.
(11) Baxter, A.; Dillon, M.; Taylor, A.; Roberts, G. A. F. *Int. J. Biol. Macromol.* **1992**, *14*, 166.
(12) Vachoud, L.; Zydowicz, N.; Domard, A. *Carbohydr. Res.* **1997**, *302*, 169.
(13) Dubuisson, J. M.; Dauvergne, J. M.; Depautex, C.; Vachette, P.; Williams, C. *Nucl. Instrum. Methods Phys. Res.* **1986**, *A286*, 636.
(14) Imperor-Clerc, M.; Davidson, P. *Eur. Phys. J. B* **1999**, *9*, 93.
(15) Oldenburg, R.; Wen, X.; Meyer, R. B.; Caspar, D. L. D. *Phys. Rev. Lett.* **1988**, *61*, 1851.
(16) Purdy, K. R.; Dogic, Z.; Fraden, S.; Ruhm, A.; Lurio, L.; Mochrie, S. G. *Phys. Rev. E* **2003**, *67*, 031708.
(17) Dadmun, M. D.; Han, C. C. *Macromolecules* **1994**, *27*, 7522.

(18) Keates, P.; Mitchell, G. R.; Peuvrel-Disdier, E.; Navard, P. *Polymer* **1993**, *34*, 1317.
(19) Villeti, M.; Borsali, R.; Diat, O.; Soldi, V.; Fukada, K. *Macromolecules* **2000**, *33*, 9418.
(20) Picken, S. J.; Aerts, J.; Visser, R.; Northolt, M. G. *Macromolecules* **1990**, *23*, 3849.
(21) Davidson, P.; Bourgaux, C.; Schoutteten, L.; Sergot, P.; Williams, C.; Livage, J. *J. Phys. II* **1995**, *5*, 1577.
(22) Maier, E. E.; Krause, R.; Deggelmann, M.; Hagenbuchle, M.; Weber, R.; Fraden, S. *Macromolecules* **1992**, *25*, 1125.
(23) Keates, P.; Mitchell, G. R.; Peuvrel, E. *Polymer* **1992**, *33*, 3298.
(24) Borsali, R.; Rinaudo, M.; Noirez, L. *Macromolecules* **1995**, *28*, 1085.
(25) Leadbetter, A. J.; Norris, E. K. *Mol. Phys.* **1979**, *38*, 669.
(26) Davidson, P.; Petermann, D.; Levelut, A. M. *J. Phys. II* **1995**, *5*, 113.
(27) Maier, W.; Saupe, A. *Z. Naturforsch.* **1958**, *13a*, 564.
(28) Maier, W.; Saupe, A. *Z. Naturforsch.* **1959**, *14a*, 882.
(29) Maier, W.; Saupe, A. *Z. Naturforsch.* **1960**, *15a*, 287.
(30) Onsager, L. *Ann. N. Y. Acad. Sci.* **1949**, *51*, 627.
(31) Vroege, G. J.; Lekkerkerker, H. N. W. *Rep. Prog. Phys.* **1992**, *55*, 1241.
(32) Nge, T. T.; Hori, N.; Takemura, A.; Ono, H. *Langmuir* **2003**, *19*, 1390.
(33) Nge, T. T.; Hori, N.; Takemura, A.; Ono, H.; Kimura, T. *J. Polym. Sci. Part B* **2003**, *41*, 711.
(34) Sugiyama, J.; Chanzy, H.; Maret, G. *Macromolecules* **1992**, *25*, 4232.
(35) Revol, J. F.; Godbout, L.; Dong, X. M.; Chanzy, H.; Maret, G. *Liq. Cryst.* **1994**, *16*, 127.
(36) Lee, S.-D. *J. Chem. Phys.* **1987**, *87*, 4972.
(37) Aubouy, M.; Trizac, E.; Bocquet, L. *J. Phys. A: Math. Gen.* **2003**, *36*, 5835.
(38) Fraden, S.; Maret, G.; Caspar, D. L. D.; Meyer, R. *Phys. Rev. Lett.* **1989**, *63*, 2068.
(39) Borgstrom, J.; Egermayer, M.; Sparrman, T.; Quist, P. O.; Piculell, L. *Langmuir* **1998**, *14*, 4935.
(40) Rouault, Y.; Iliopoulos, I.; Audebert, R. *Polym. Bull.* **1997**, *39*, 741.
(41) Cheng, S. Z. D.; Lee, S. K.; Barley, J. S.; Hsu, S. L. C.; Harris, F. W. *Macromolecules* **1991**, *24*, 1883.
(42) Terech, P.; Weiss, R. G. *Chem. Rev.* **1997**, *97*, 3133.
(43) Mourchid, A.; Delville, A.; Lambard, J.; Lécolier, E.; Levitz, P. *Langmuir* **1995**, *11*, 1942.
(44) Gabriel, J. C. P.; Sanchez, C.; Davidson, P. *J. Phys. Chem.* **1996**, *100*, 11139.
(45) Davidson, P.; Bourgaux, C.; Schoutteten, L.; Sergot, P.; Williams, C.; Livage, J. *J. Phys. II (France)* **1995**, *5*, 1577.
(46) van Bruggen, M. P. B.; Lekkerkerker, H. N. W. *Langmuir* **2002**, *18*, 7141.
(47) van der Beek, D.; Lekkerkerker, H. N. W. *Europhys. Lett.* **2003**, *61*, 702.
(48) Zocher, H.; Jacobsohn, K. *Kolloidchem. Beih.* **1929**, *28*, 167.
(49) Buining, P. A.; Philipse, A. P.; Lekkerkerker, H. N. W. *Langmuir* **1994**, *10*, 2106.
(50) Wierenga, A.; Philipse, A. P.; Lekkerkerker, H. N. W. *Langmuir* **1998**, *14*, 55.
(51) Philipse, A. P. *Langmuir* **1996**, *12*, 1127.
(52) Philipse, A. P.; Wierenga, A. M. *Langmuir* **1998**, *14*, 49.
(53) Buitenhuis, J.; Donselaar, L. N.; Buining, P. A.; Stroobants, A.; Lekkerkerker, H. N. W. *J. Colloid Interface Sci.* **1995**, *175*, 46.
(54) Straley, J. P. *Phys. Rev.* A **1976**, *14*, 1835.
(55) Odijk, T. *J. Phys. Chem.* **1987**, *91*, 6060.
(56) Pelcovits, R. *Liq. Cryst.* **1996**, *21*, 361.
(57) Kornyshev, A. A.; Leikin, S. *Phys. Rev. E* **2000**, *62*, 2576.
(58) Kornyshev, A. A.; Leikin, S.; Malinin, S. V. *Eur. Phys. J.* **2002**, *E7*, 83.
(59) Dogic, Z.; Fraden, S. *Langmuir* **2000**, *16*, 7820.
(60) Van Winkle, D. H.; Davidson, M. W.; Chen, W. X.; Rill, R. L. *Macromolecules* **1990**, *23*, 4140.
(61) Livolant, F. *J. Phys.* **1986**, *47*, 1605.
(62) Robinson, C. *Tetrahedron* **1961**, *13*, 219.
(63) Grelet, E.; Fraden, S. *Phys. Rev. Lett.* **2003**, *90*, 198302−1.
(64) Sato, T.; Teramoto, A. *Physica A* **1991**, *176*, 72.
(65) Manning, G. S. *J. Chem. Phys.* **1969**, *51*, 924.